

Supporting Information:

**Pathway Dependent Preferential Selection and Amplification of
Variable Self-Assembled Peptide Nanostructures and their
Biological Activity**

Harsimran Kaur, Rashmi Jain and Sangita Roy*

Institute of Nano Science and Technology, Phase-10, Sector-64, Mohali, Punjab-160062, India.

Table of Contents:

Table and figures

Table S1: Optical images of the Cbz-FF-OH hydrogels formed by pathway I and II in phosphate buffer (pH 8.0) of different concentrations.

Table S2: Zeta potential values of the Cbz-FF-OH hydrogels formed by pathway I and II.

Figure S1. TEM and SEM images of the Cbz-FF-OH hydrogel formed by pathway I and II.

Figure S2. Spectra representing the variation in HT with wavelength during CD measurement of Cbz-FF-OH hydrogels formed by pathway I and II in phosphate buffer (pH 8.0) with different ionic strength.

Figure S3. (a, b) Thioflavin T binding assays and (c, d) molecular rotor study performed with Cbz-FF-OH hydrogels formed by pathway I and II, respectively.

Figure S4. Fluorescence emission and UV- visible absorption spectra of the Cbz-FF-OH hydrogels formed by pathway I and II.

Figure S5. Congo red (CR) binding assay of the Cbz-FF-OH hydrogels formed by a) pathway I and b) pathway II, respectively. c) Plot showing red shift in the absorption maxima of CR dye on the formation of nanostructures in the hydrogels.

Figure S6. a) Comparison of average diameter of nanostructures and b) storage modulus of the Cbz-FF-OH hydrogels formed by pathway I and II, respectively.

Figure S7. Assessment of the mechanism of formation of differential nanostructures through on- and off-pathway. a) Schematic representation and b) CD analysis of transition process involve in the thermo-reversibility study of the kinetically trapped structures of pathway II gel. c) Spectra representing the variation in HT with wavelength during the transition process of the kinetically trapped structures of pathway II gel to the thermodynamically favoured structures.

Figure S8: Time dependent AFM and rheology studies of the pathway II gel formed in 50 mM phosphate buffer (pH 8.0).

Figure S9: AFM images of the DMEM diluted hydrogels, gel I formed by pathway I and gel II formed by pathway II used as treatment during MTT assay.

Figure S10. Microscopic images of the CHO, NIH3T3 and L929 cell lines after 4 h treatment with 1000 µg/ml of gel I, and gel II.

Figure S11: Cell viability of L929 cell line after 4 h treatment with different concentration of Cbz-FF-OH hydrogels formed through pathway I and pathway II in 75 mM, and 100 mM of phosphate buffer (pH 8.0).

Figure S12: Comparison of cellular viability of L929 cell line after 4 h treatment with 1000 µg/ml of Cbz-FF-OH hydrogels formed through pathway I and pathway II in 50 mM, 75 mM, and 100 mM concentration of phosphate buffer (pH 8.0).

Figure S13: a) Cell viability of L929 cell line after 4 h treatment with different concentration of Cbz-FF-OH hydrogels formed after heating the pathway II gel during thermo-reversibility study.

Figure S14: Quantification of cellular viability and proliferation of L929 cell line on Cbz-FF-OH (30 mM) hydrogels formed by pathway I and II in 50 mM phosphate buffer (pH 8.0).

Table S1: Optical images of the Cbz-FF-OH hydrogels formed by pathway I and II in phosphate buffer (pH 8.0) of concentration 50 mM, 75 mM and 100 mM respectively.

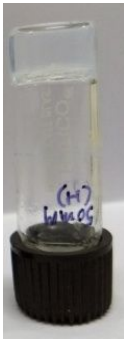
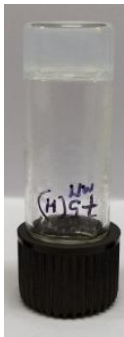
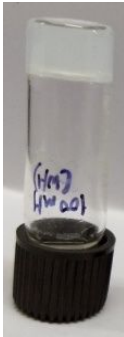
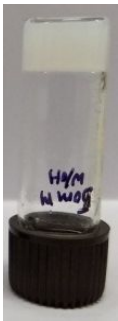
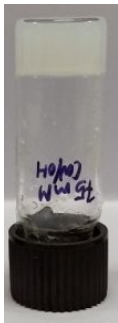
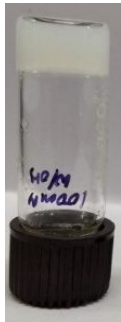
Pathways of synthesis	Concentration of phosphate buffer (pH 8.0)		
	50 mM	75 mM	100 mM
Pathway I	Gel I (50 mM) 	Gel I (75 mM) 	Gel I (100 mM) 
Pathway II	Gel II (50 mM) 	Gel II (75 mM) 	Gel II (100 mM) 

Table S2: Zeta potential values of the Cbz-FF-OH (30 mM) hydrogels formed by pathway I and II in 50 mM phosphate buffer (pH 8.0).

Cbz-FF-OH hydrogel	Gel I	Gel II
Zeta Potential values (mV)	-40.6± 2.72	-46.7± 3.27

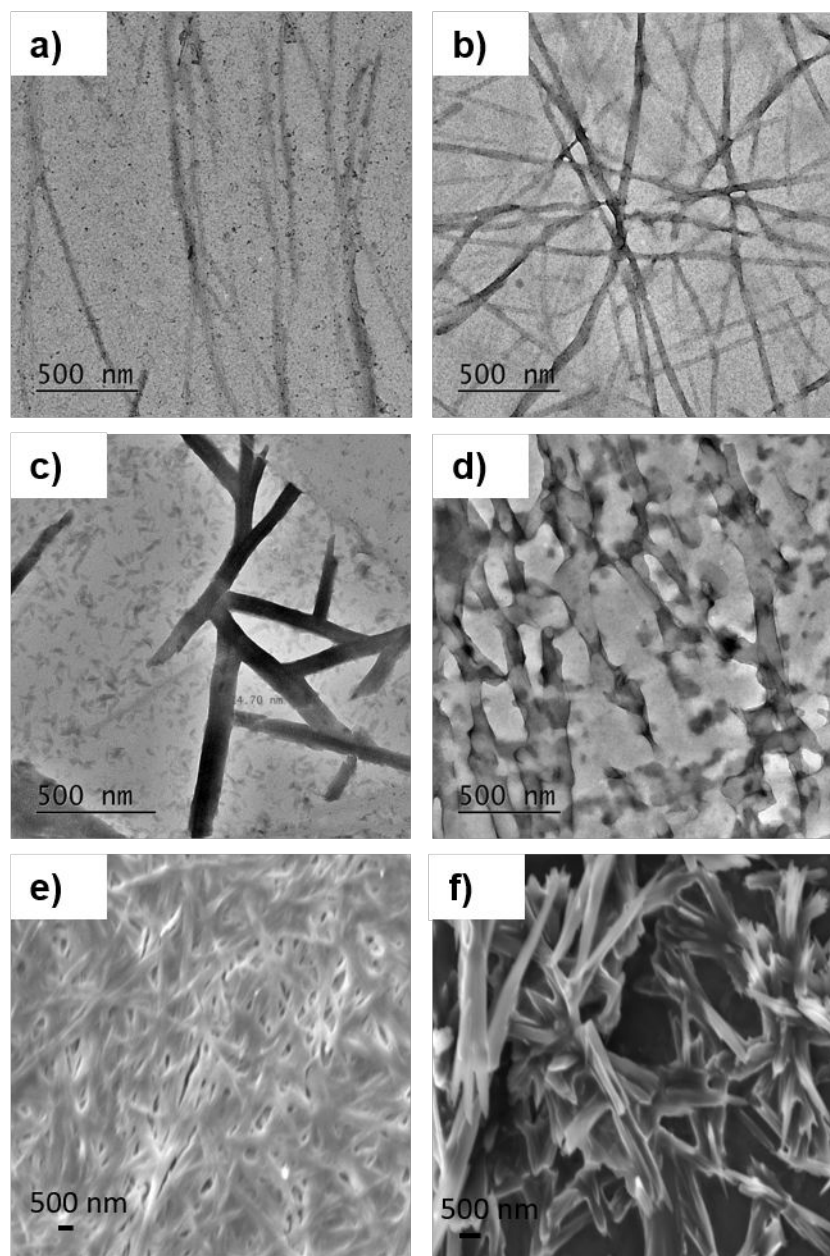


Figure S1: TEM images of the Cbz-FF-OH hydrogel formed by pathway I in phosphate buffer (pH 8.0) of concentration (a) 50 mM, (b) 100 mM and by pathway II in phosphate buffer (pH 8.0) of concentration (c) 50 mM and (d) 100 mM. SEM images of the Cbz-FF-OH hydrogel formed by e) pathway I and f) pathway II in 50 mM phosphate buffer (pH 8.0).

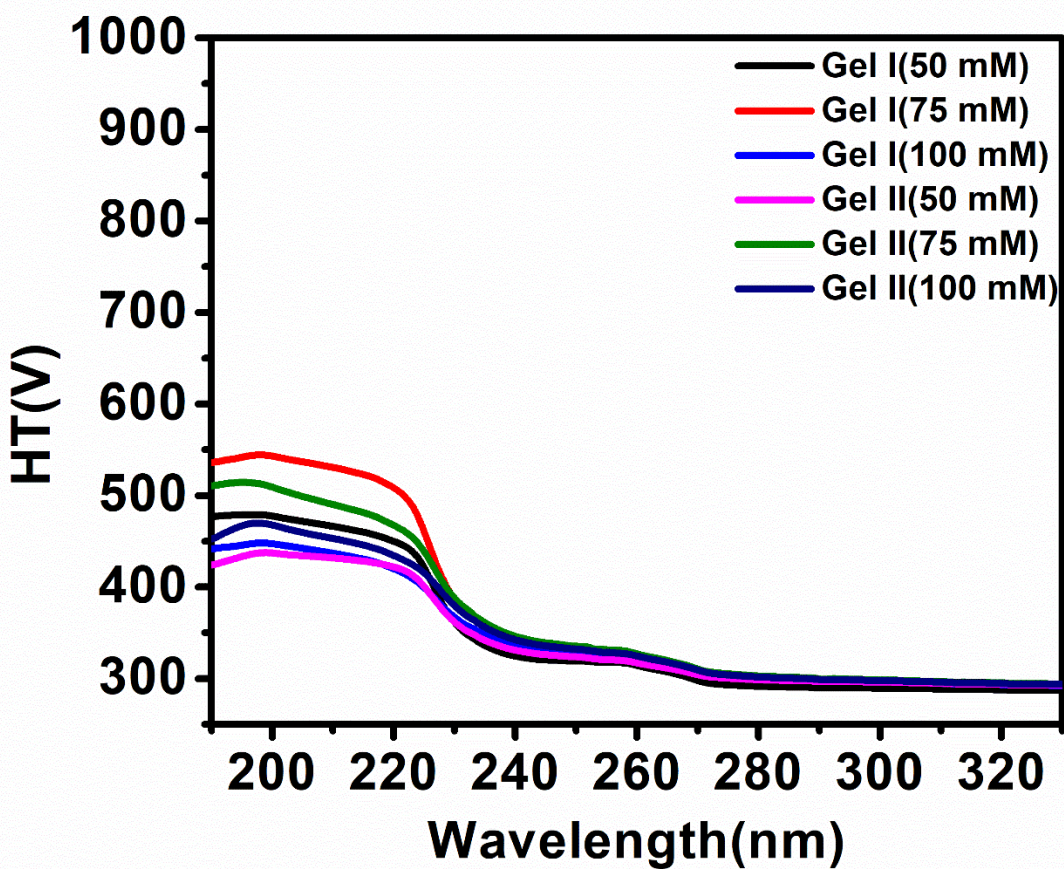


Figure S2: Spectra showing the variation in HT voltage with wavelength during CD spectroscopic analysis of Cbz-FF-OH hydrogels, Gel I and Gel II, formed in different concentration of phosphate buffer (pH 8.0) 50 mM, 75 mM, and 100 mM.

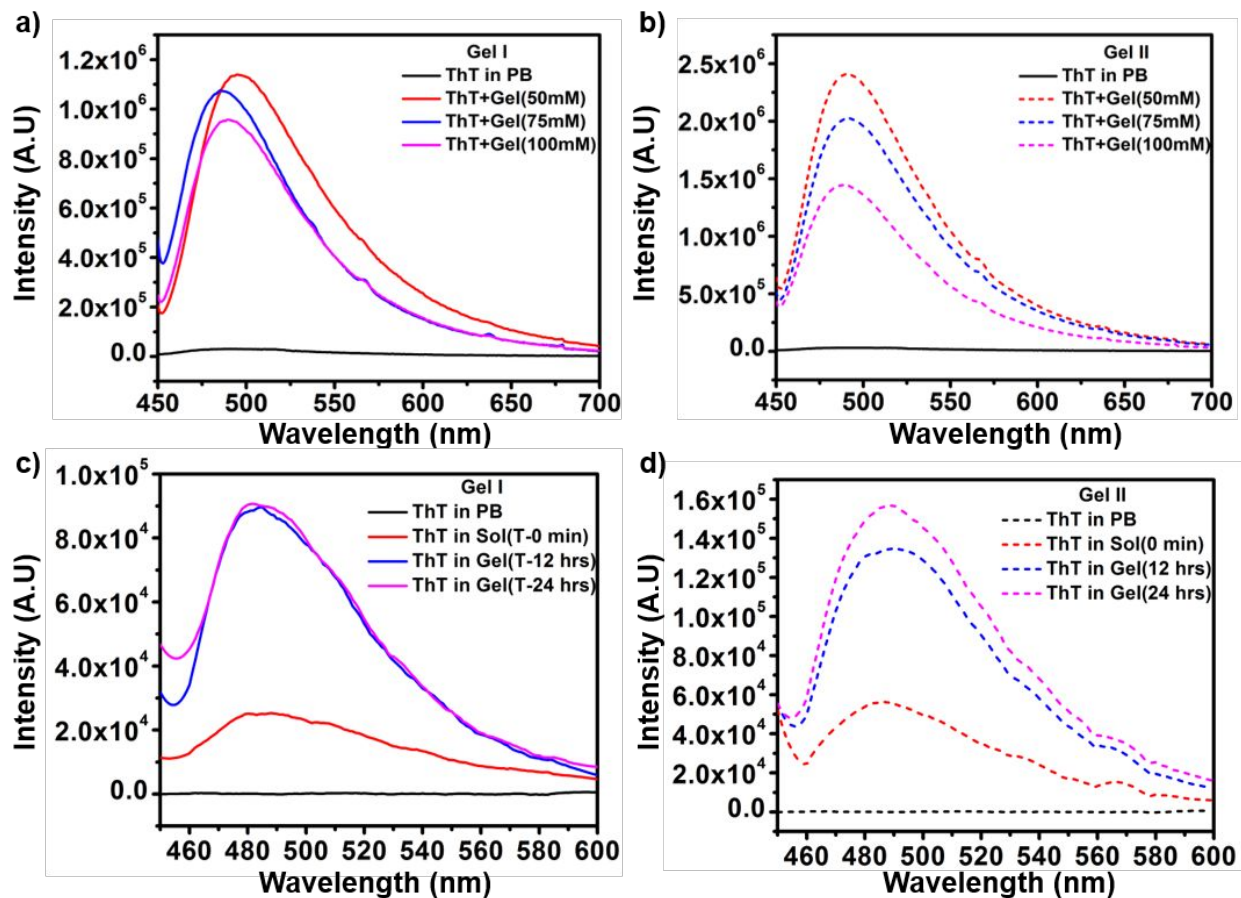


Figure S3: Thioflavin T binding assays performed with Cbz-FF-OH hydrogels formed in different concentration of phosphate buffer (pH 8.0) i.e., 50 mM, 75 mM, and 100 mM through a) pathway I and b) pathway II. Molecular rotor study through fluorescence emission of Thioflavin T in Cbz-FF-OH hydrogels formed in 50 mM phosphate buffer (pH 8.0) through c) Pathway I and d) Pathway II.

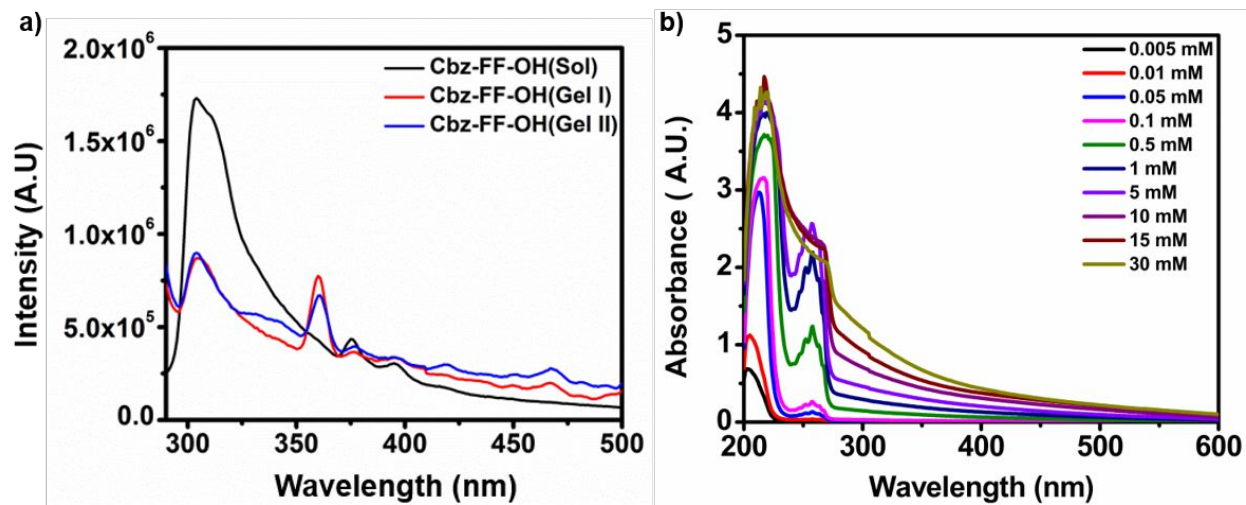


Figure S4: a) Fluorescence emission spectra of the Cbz-FF-OH hydrogels formed by pathway I and II in 50 mM phosphate buffer (pH 8.0). b) UV- Visible absorption spectra of the Cbz-FF-OH at different concentrations in 50 mM phosphate buffer (pH 8.0).

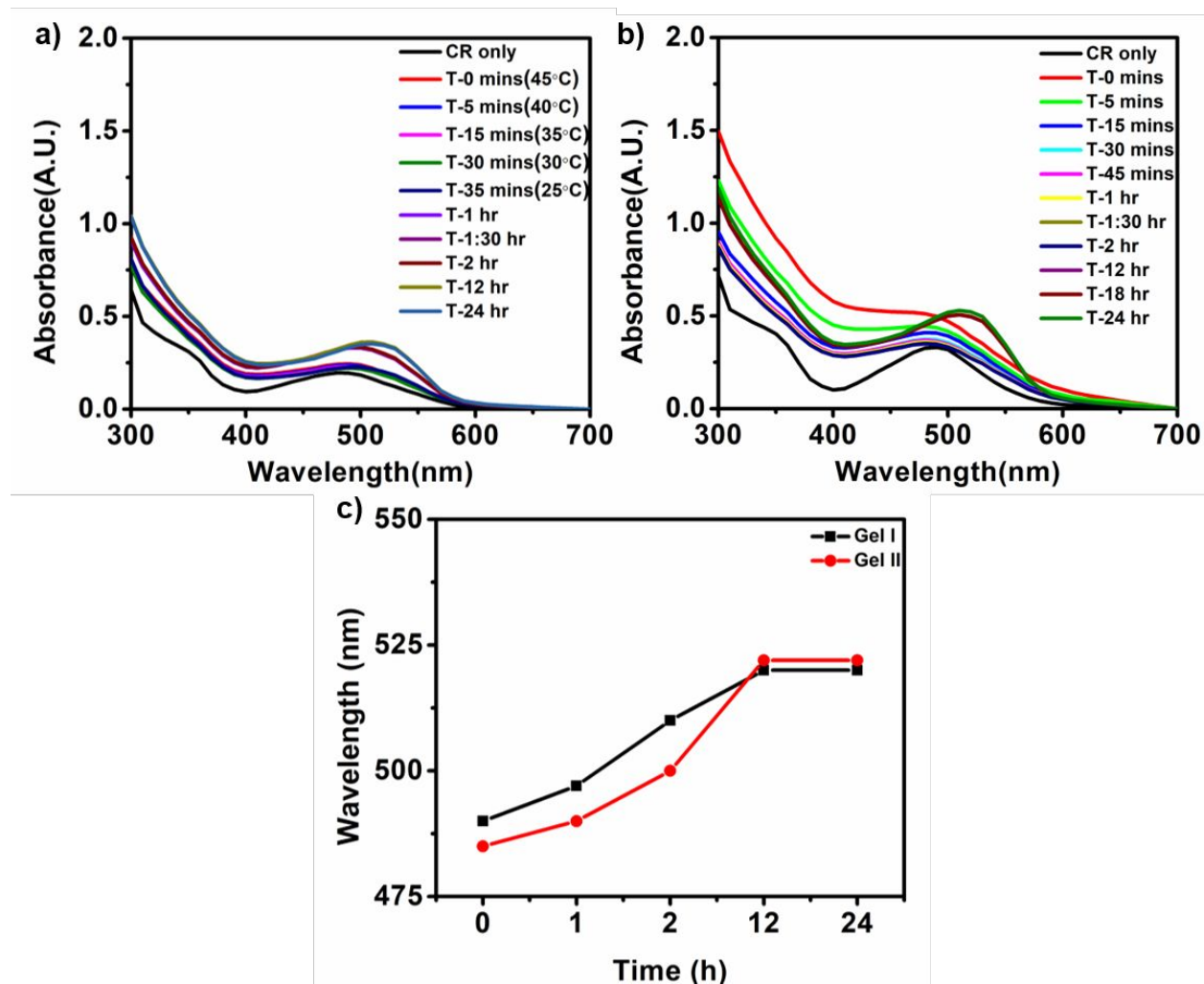


Figure S5: Congo red (CR) binding assay of (a) gel I and (b) gel II formed by pathway I and II, respectively. For pathway I gel, at initial time points the peptide solution still remains at higher temperature and was allowed to cool to room temperature thus initial time points were taken at different temperatures showing gradual temperature decrease to room temperature. Whereas in pathway II gel, after sonication the peptide solution was kept undisturbed at room temperature thus different time points were taken at room temperature. c) Graph showing red shift of the absorption maximum of CR dye from 490 nm to 520 nm on binding to the nanostructures formed during gelation by pathway I and II in 50 mM phosphate buffer (pH 8.0).

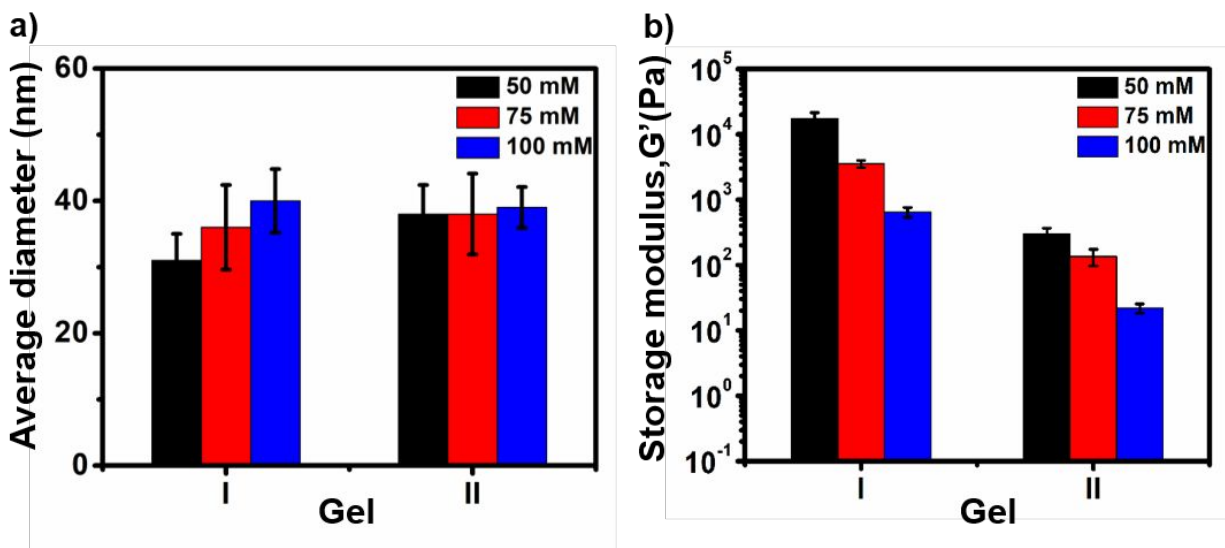


Figure S6: a) Comparison of average diameter of nanostructures of the gel I and gel II formed by pathway I and pathway II, respectively, with different concentration of phosphate buffer (pH 8.0) 50 mM, 75 mM and 100 mM. b) Comparison of storage modulus of the gel I and gel II formed by pathway I and pathway II respectively, with different concentration of phosphate buffer (pH 8.0) 50 mM, 75 mM, and 100 mM.

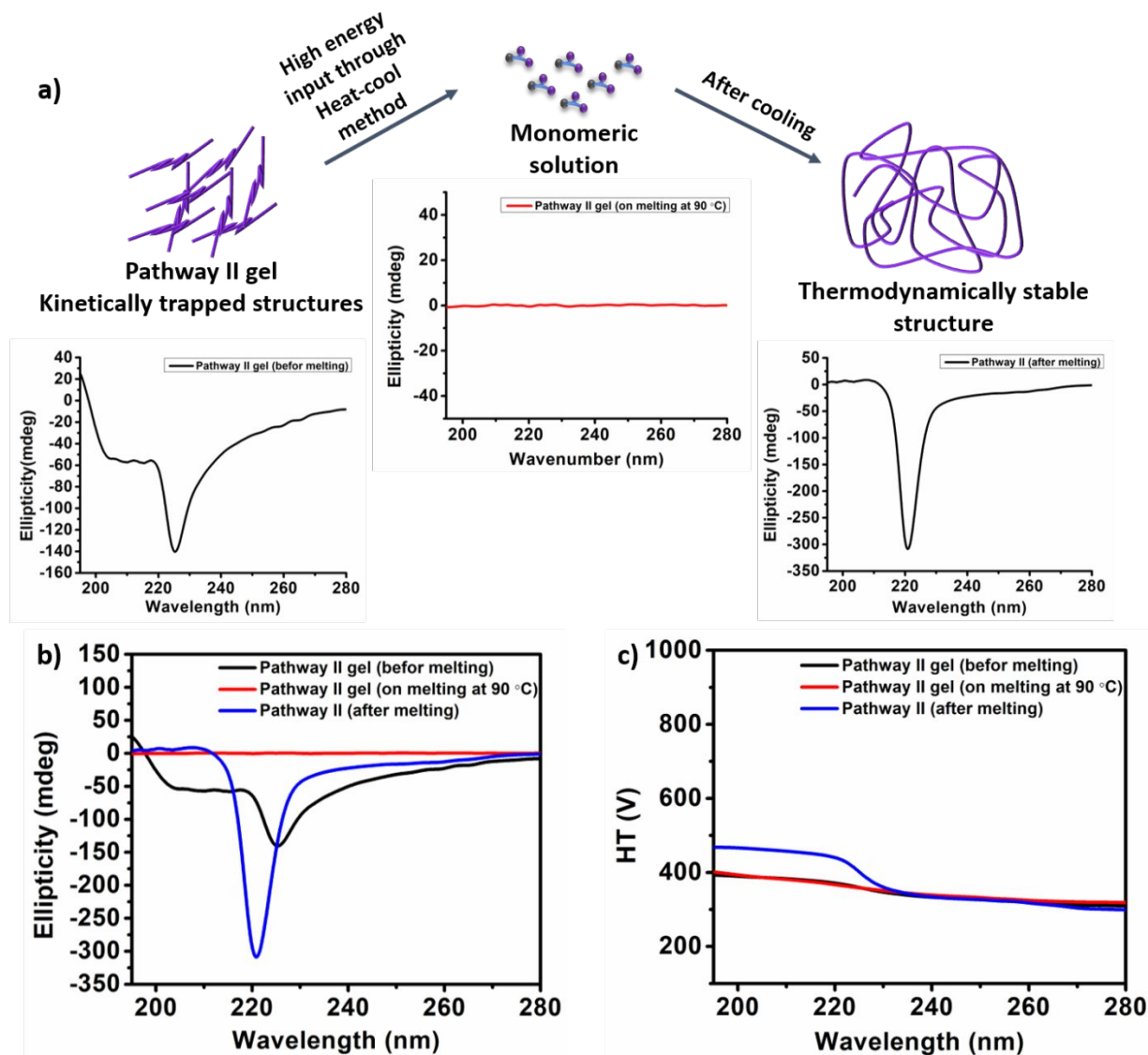


Figure S7: Assessment of the mechanism of formation of differential nanostructures through on- and off-pathway. a) Schematic representation of transition process involves in the thermo-reversibility study where the kinetically trapped structures are the off-pathway product of the final thermodynamically favoured structures. b) CD analysis during the thermo-reversibility study of Cbz-FF-OH hydrogel formed by pathway II in 50 mM phosphate buffer (pH 8.0) before, after and on melting the gel at 90 °C. c) Spectra showing the variation in HT voltage with wavelength during CD spectroscopic measurement for Cbz-FF-OH hydrogel at different stages of thermo-reversibility study.

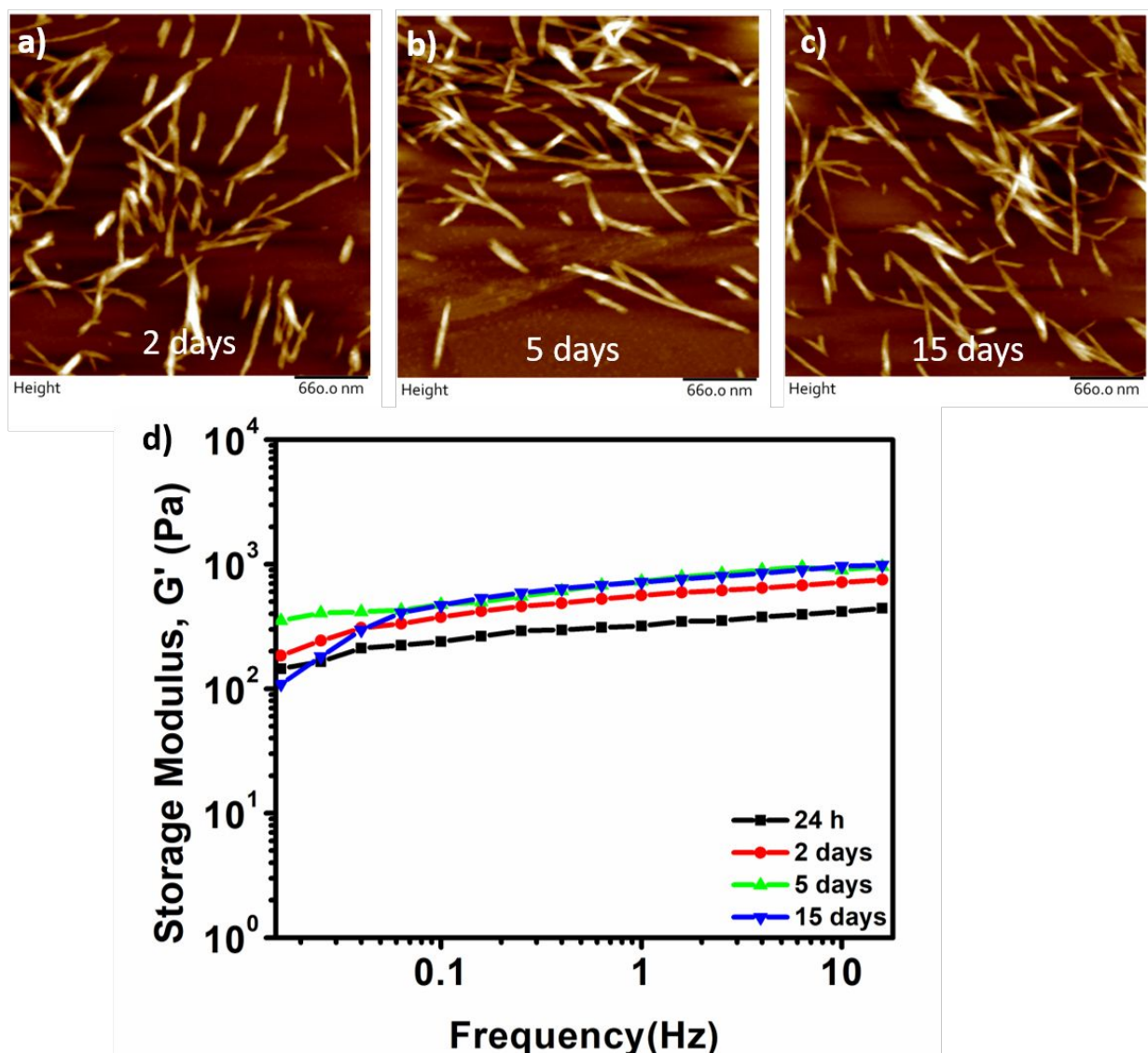


Figure S8: Time dependent AFM and rheology studies of the pathway II gel formed in 50 mM phosphate buffer (pH 8.0). AFM height image of gel II after a) 2 days, b) 5 days, and c) 15 days of incubation. The Z scale of the AFM images are following: a) 0-38.7 nm, b) 0-31.7 nm, and c) 0-41.6 nm. d) The mechanical strength analysis of gel II formed in 50 mM phosphate buffer (pH 8.0) over different time points 24 h, 2 days, 5 days, and 15 days.

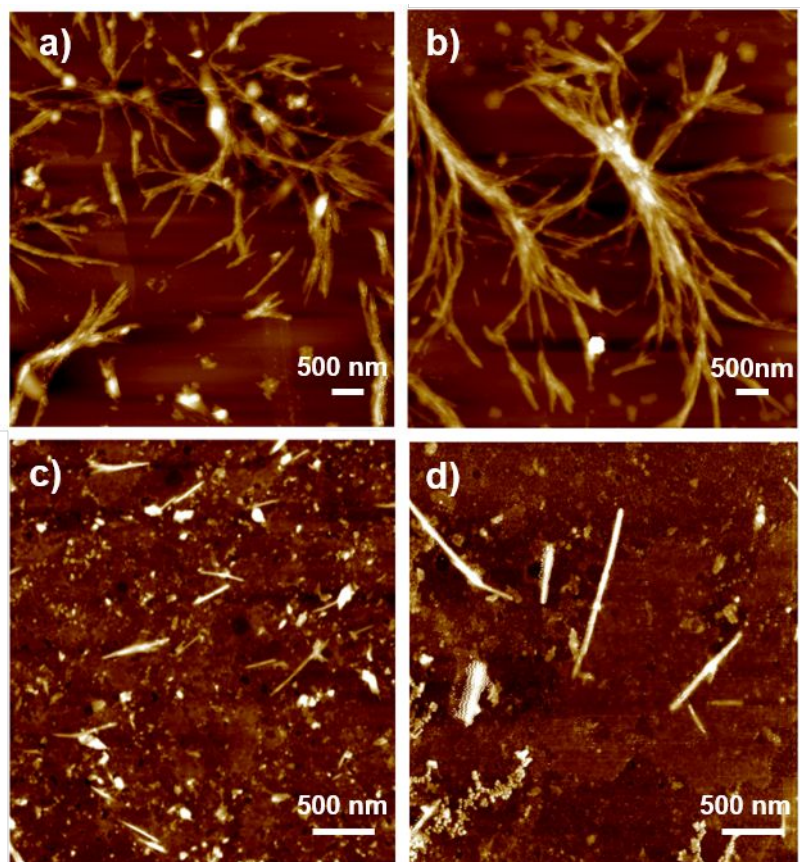


Figure S9: AFM height images of gel I and gel II diluted in DMEM media with final concentration (a, c) 500 $\mu\text{g/ml}$ and (b, d) 1000 $\mu\text{g/ml}$ used as treatment during MTT assay. The Z scale of the AFM images are following: a) 0-61.0 nm, b) 0-58.5 nm, c) 0-45.7 nm, and d) 0-50.3 nm.

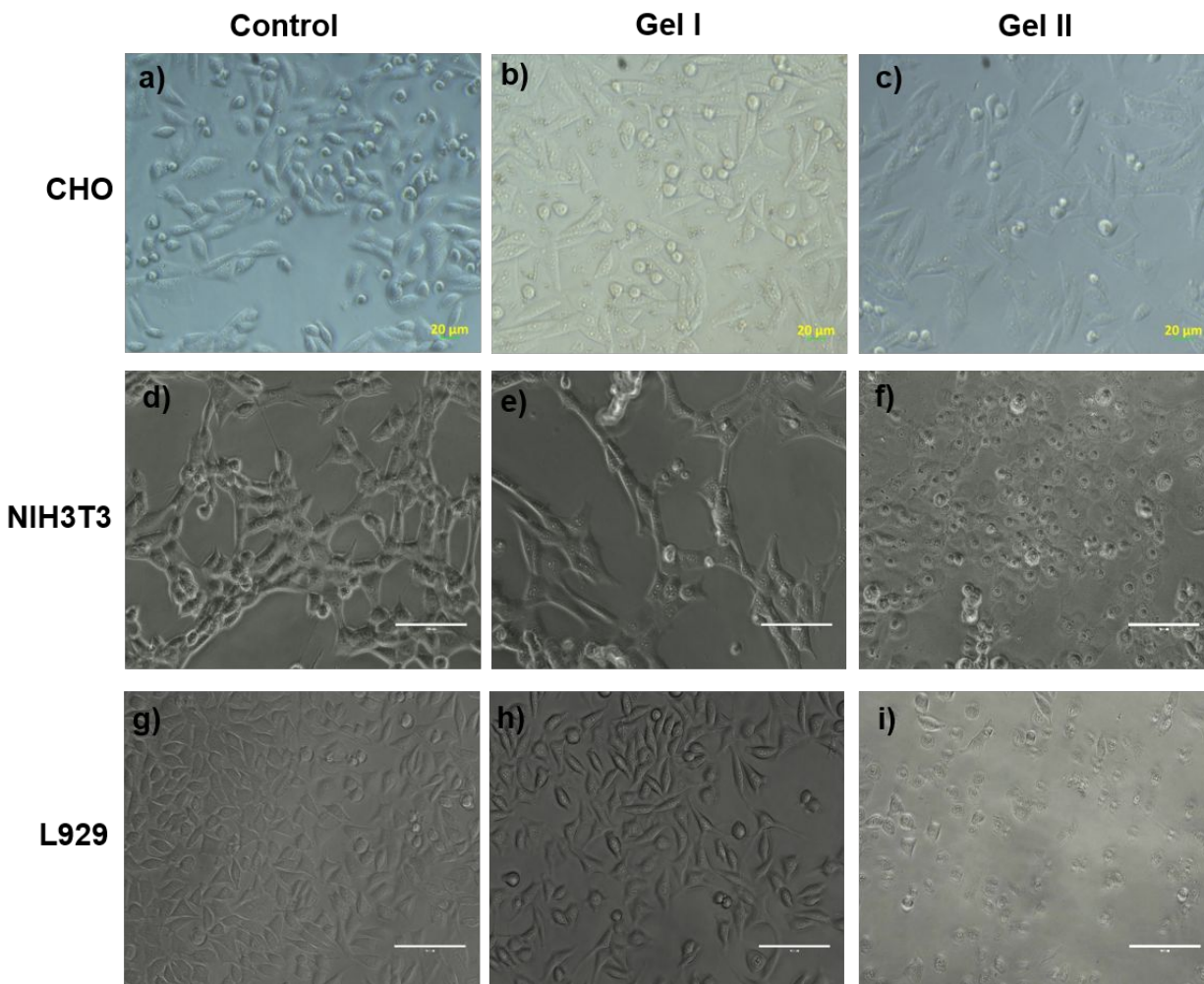


Figure S10: Microscopic images of the CHO(a-c), NIH3T3(d-f) and L929(g-i) cell lines. Cell culture images of (a, d, g) control, (b, e, h) treated with 1000 $\mu\text{g/ml}$ of gel I formed by pathway I, (c, f, i) treated with 1000 $\mu\text{g/ml}$ of gel II formed by pathway II after 4 h of treatment.

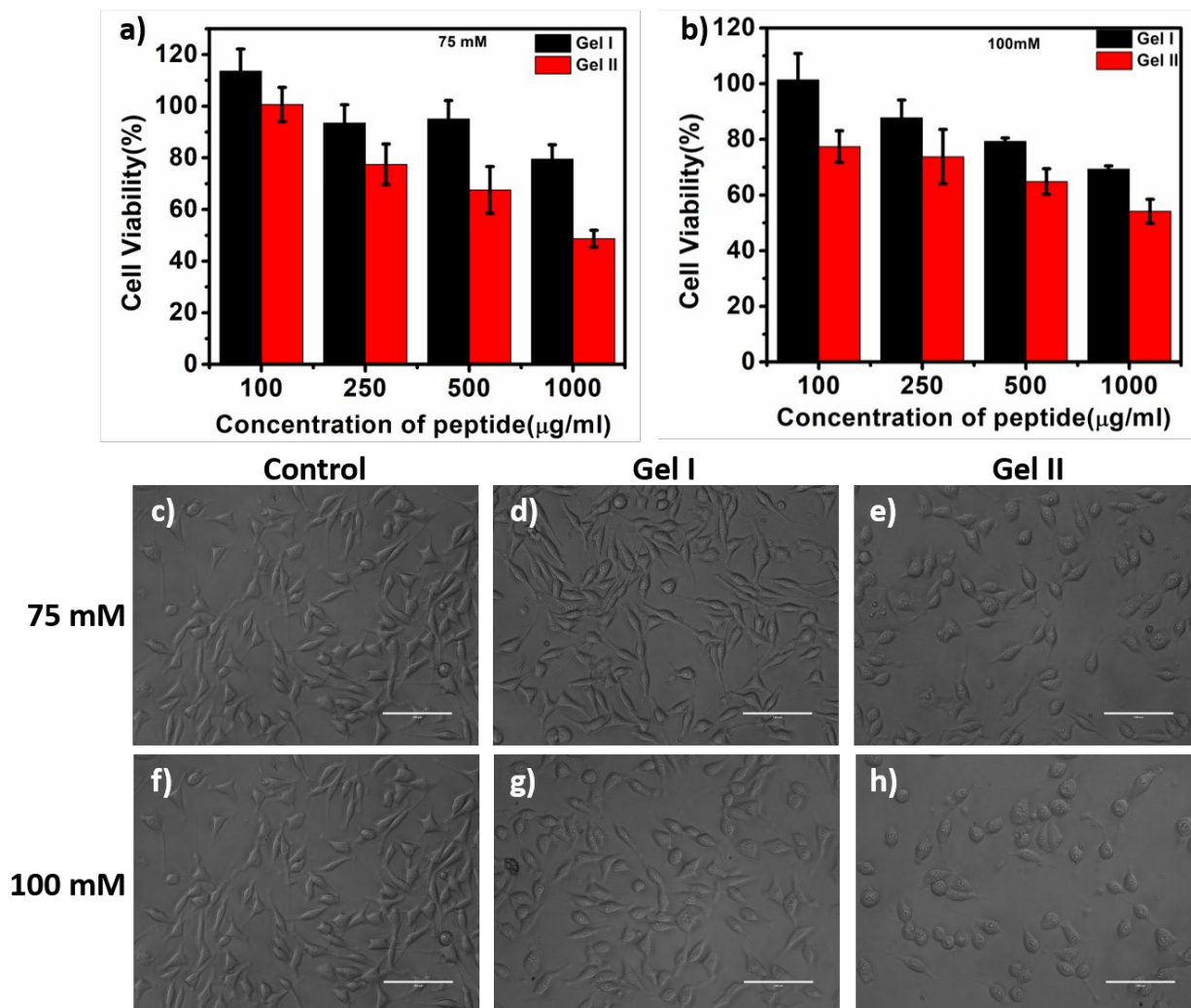


Figure S11: Cell viability of L929 cell line after 4 h treatment with different concentration of Cbz-FF-OH hydrogels formed through pathway I and pathway II in (a) 75 mM, and (b) 100 mM of phosphate buffer (pH 8.0). Microscopic images of the L929 cells (c, f) control, (d, g) when treated with 1000 µg/mL of gel I and (e, h) when treated with 1000 µg/mL of gel II formed in 75 mM and 100 mM of phosphate buffer (pH 8.0) for 4 h. Scale bar is 100 µm.

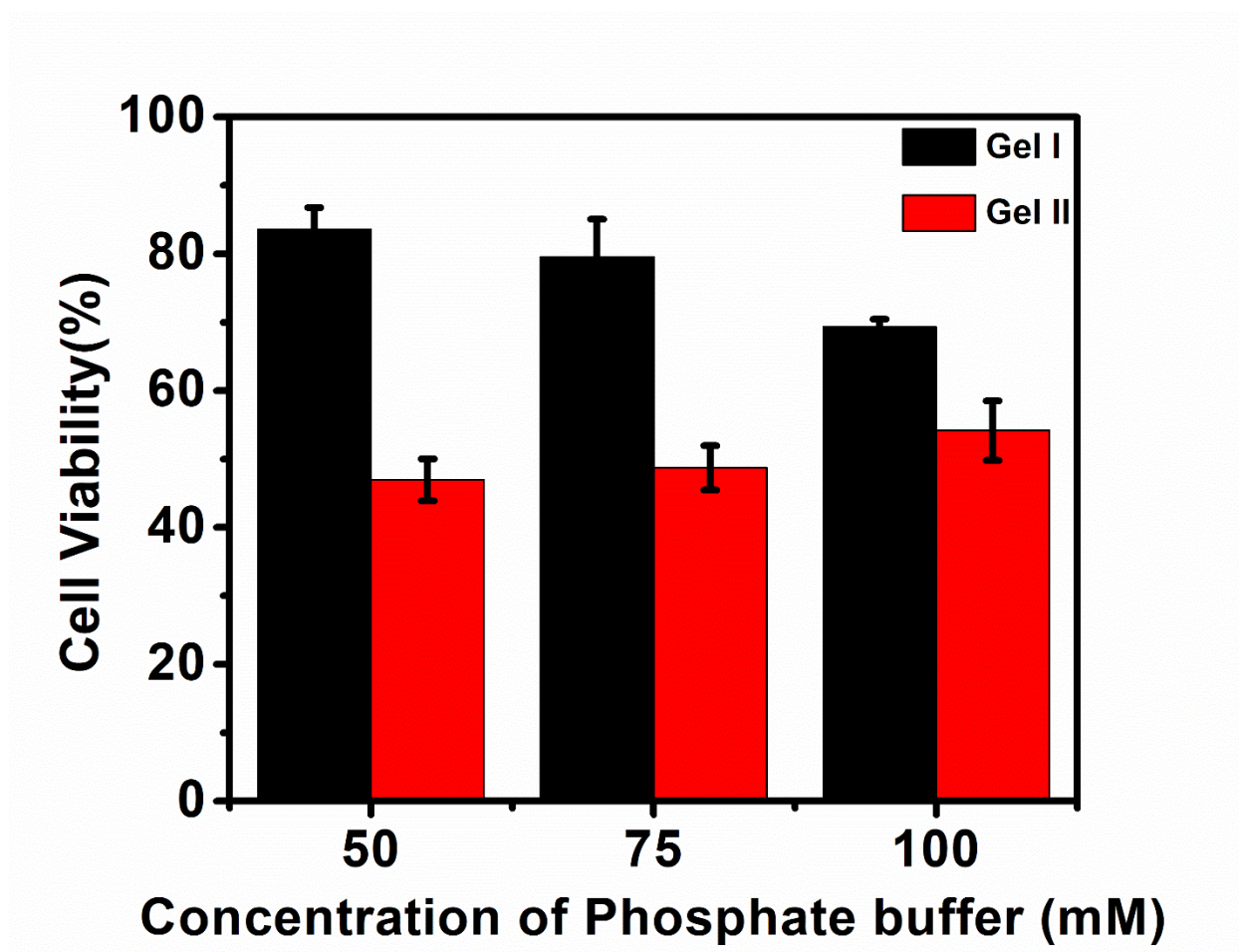


Figure S12: Comparison of cellular viability of L929 cell line after 4 h treatment with 1000 µg/ml of Cbz-FF-OH hydrogels formed through pathway I and pathway II in 50 mM, 75 mM, and 100 mM concentration of phosphate buffer (pH 8.0).

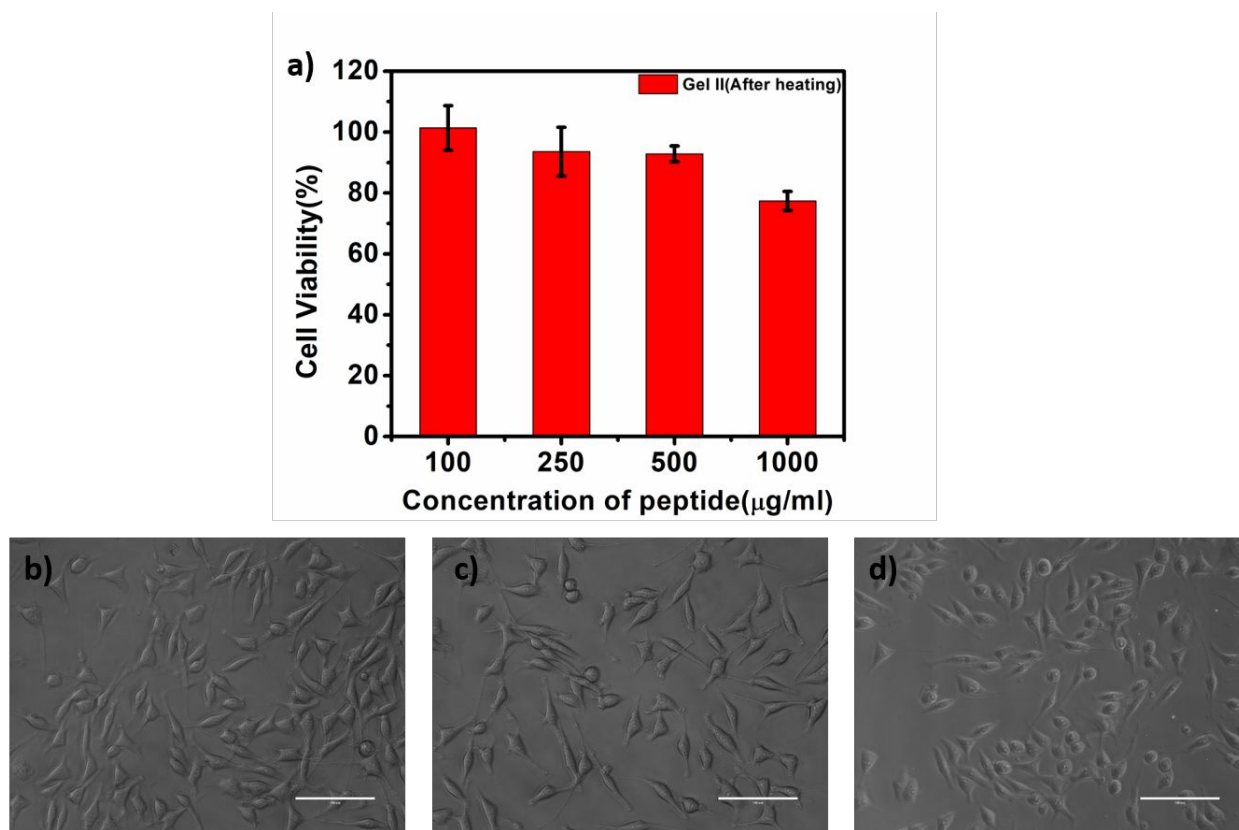


Figure S13: a) Cell viability of L929 cell line after 4 h treatment with different concentration of Cbz-FF-OH hydrogels formed after heating the pathway II gel during thermo-reversibility study. Microscopic images of the L929 cells (b) control, (c) when treated with 500 μg/mL, and (d) when treated with 1000 μg/mL of gel formed after heating pathway II gel for 4 h. Scale bar is 100 μm.

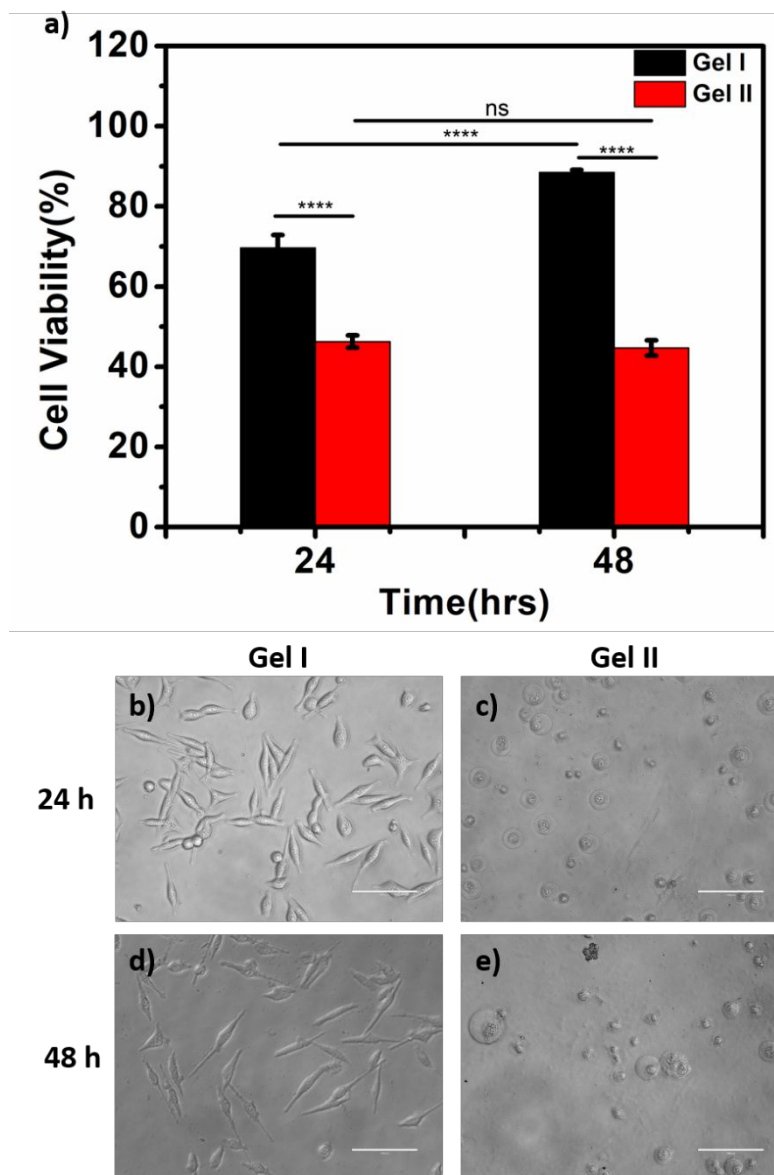


Figure S14: Quantification of cellular viability and proliferation of (a) mouse fibroblast cell line, L929 on Cbz-FF-OH (30 mM) hydrogels formed by pathway I and II in 50 mM phosphate buffer (pH 8.0) using MTT assay at different time points. Data are represented as mean \pm SD. **** represents P -value ≤ 0.0001 and “ns” stands for nonsignificant difference (two-way ANOVA, Bonferroni’s multiple comparisons tests). Microscopic images of L929 cells after (b, c) 24 and (d, e) 48 h incubation on Cbz-FF-OH hydrogels (Gel I and Gel II). Scale bar is 100 μ m.